JACS
JOURNAL OF THE AMERICAN CHEMICAL SOCIETY
Article
pubs.acs.org/JACS

Electrochemical Insight into the Brust–Schiffrin Synthesis of Au Nanoparticles

Akihiro Uehara,[*,†,‡] Samuel G. Booth,[‡] Sin Yuen Chang,[§] Sven L. M. Schroeder,[⊥] Takahito Imai,[#] Teruo Hashimoto,[∥] J. Frederick W. Mosselmans,[▽] and Robert A. W. Dryfe[‡]

[†]Division of Nuclear Engineering Science, Research Reactor Institute, Kyoto University, Asashironishi, Kumatori, Osaka 590-0494, Japan

[‡]School of Chemistry, [§]School of Chemical Engineering and Analytical Science, and [∥]School of Materials, The University of Manchester, Oxford Road, Manchester M13 9PL, United Kingdom

[⊥]School of Chemical and Process Engineering, Faculty of Engineering, University of Leeds, Leeds LS2 9JT, United Kingdom

[#]Department of Materials Chemistry, Faculty of Science and Technology, Ryukoku University, Otsu, Shiga 520-2194, Japan

[▽]Diamond Light Source Ltd, Didcot, Oxfordshire OX11 0DE, United Kingdom

Supporting Information

ABSTRACT: The mechanism of the Brust–Schiffrin gold nanoparticle synthesis has been investigated through the use of ion transfer voltammetry at the water/1,2-dichloroethane (DCE) solution interface, combined with X-ray absorption fine structure (XAFS) of the reaction between $[AuCl_4]^-$ and thiol (RSH) in homogeneous toluene (TL) solution. Ion transfer calculations indicate the formation of $[AuCl_2]^-$ at RSH/Au ratios from 0.2–2 with a time-dependent variation observed over several days. At RSH/Au ratios above 2 and after time periods greater than 24 h, the formation of Au(I)SR is also observed. The relative concentrations of reaction products observed at the liquid/liquid interface are in excellent agreement with those observed by XAFS for the corresponding reaction in a single homogeneous phase. BH_4^- ion transfer reactions between water and DCE indicate that the reduction of $[AuCl_4]^-$ or $[AuCl_2]^-$ to Au nanoparticles by BH_4^- proceeds in the bulk organic phase. On the other hand, BH_4^- was unable to reduce the insoluble $[Au(I)SR]_n$ species to Au nanoparticles. The number and size of the nanoparticles formed was dependent on the concentration ratio of RSH/Au, as well as the experimental duration because of the competing formation of the $[Au(I)SR]_n$ precipitate. Higher concentrations of nanoparticles, with diameters of 1.0–1.5 nm, were formed at RSH/Au ratios from 1 to 2.

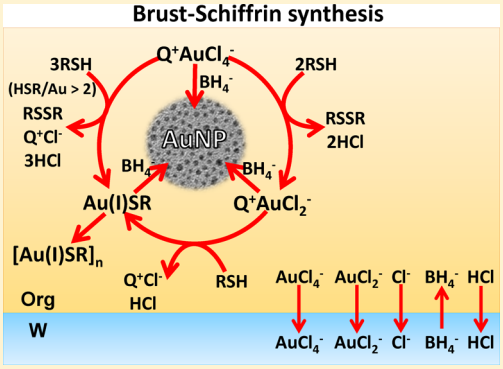

INTRODUCTION

The Brust–Schiffrin method is the earliest reported phase transfer approach to prepare thiol-stabilized metal nanoparticles.[1] In this two-step approach, the gold ions from an aqueous solution are first extracted to a hydrocarbon (e.g. toluene, TL) phase using tetraoctylammonium bromide, TOA^+Br^-, as the phase transfer reagent. The phase transfer of negatively charged gold ions (e.g. tetrachloroaurate ion, $[AuCl_4]^-$) to the aqueous phase proceeds by exchange with the more hydrophilic Br^- ions in the organic phase, which are present as the counterions of TOA^+. Following $[AuX_4]^-$ transfer (X = halide) to the organic phase, the aqueous solution is discarded. Subsequent reduction reactions in the organic solution, using a second aqueous solution of $NaBH_4$ in the presence of an alkanethiol added as a capping agent, yield Au nanoparticles of ~2.5 nm diameter. Although the Brust–Schiffrin method is extensively used and has been studied widely,[2−8] the synthesis process and associated mechanistic features have only recently been investigated in detail. One of the specific questions has been the identification of the precursor species present in solution prior to reduction with $NaBH_4$. In early studies of the Brust–Schiffrin process, when the precursor question was addressed, researchers generally assumed the formation of Au(I) thiolate polymers[9,10] in both the one- and two-phase reactions, with evidence that the thiol species also functioned as reducing agents, forming Au(I) from Au(III).[3] Recently, a revised view of Brust–Schiffrin nanoparticle syntheses has been pioneered by Goulet and Lennox,[11] which indicates that the thiol (RSH) behaves solely as a reductant for $[AuX_4]^-$ before the addition of $NaBH_4$, with no Au–thiol bonding observed. Au(I) reduced from Au(III) by 1-dodecanethiol was shown to be precursors of one-phase reactions conducted in organic solvents (usually TL) as in eq 1:

$$TOA^+[AuX_4]^- + 2RSH \rightleftharpoons TOA^+[AuX_2]^- + RSSR + 2HX \quad (1)$$

Received: July 27, 2015
Published: November 11, 2015

DOI: 10.1021/jacs.5b07825
J. Am. Chem. Soc. 2015, 137, 15135–15144

The product was identified based on ^{1}H NMR spectroscopy, and the mechanism was shown to proceed as above, with a further increase in the RSH/Au ratio above the stoichiometric ratio of eq 1 claimed to lead to the accumulation of free thiol in water-free organic solvents. A density functional theory calculation supported eq 1,[12] and a number of experimental studies have appeared using NMR in addition to other characterization, for example Raman spectroscopy and surface plasmon resonance, which have generally supported the veracity of eq 1.[11,13−16]

Specifically Li et al.[13,16] have clarified that the $[AuX_2]^-$ precursor in a Brust−Schiffrin two-phase synthesis is either the $TOA^+[AuX_2]^-$ complex when RSH/$[AuX_4]^-$ < 2, or a mixture of the $TOA^+[AuX_2]^-$ complex and polymeric $[Au(I)SR]_n$ species when RSH/$[AuX_4]^-$ > 2 in a two-phase system with water present. Saturation of the organic phase with water was claimed to lead to inverse micelles in the organic solvent, which were invoked to explain the size specificity of the Brust−Schiffrin process.[16] However, the existence of inverse micelles was repudiated by Perala and co-workers[17] who also developed a kinetic model based on continuous nucleation to explain the variation in particle size.[15] More recent NMR observations have indicated that the intermediate is reliant on the absolute concentration of the reactants as well as their ratio. Initial NMR observations agreed with those of Goulet and Lennox. However, on increasing the concentrations of the reactants, soluble intermediate species $TOA^+[Au(SR)X]^-$ and $TOA^+[Au(SR)_2]^-$ were also proposed,[18] the hypothesis being that the overall polarity of the solution and the pH is increased, reducing the suppression of halide liberation in the organic solvent. These soluble gold thiolate species were found to precipitate after a number of days. By performance of the reduction with thiols of different structure, it has been verified that the first two additions of thiol, required for the stoichiometric reaction, are only involved in the reduction and additional thiol may then form a bonding interaction with Au(I).[19] The formation of the polymeric $[Au(I)SR]_n$ species depends on the reaction conditions (i.e., whether there is an aqueous layer present or not): the overall deposition process has proven to be more involved than originally believed; specifically the distribution of the reactant ions and the electron transfer between water and the organic solution will depend on the interfacial potential and electroneutrality of both phases. This means that from an electrochemical point of view, we can write the Brust−Schiffrin mechanism as summarized in Figure 1: transfer of $[AuX_4]^-$ from the aqueous phase to the organic and halide ion transfer from the organic to water (process i). In some studies, Br^- is introduced as the counterion to TOA^+, and there may be some substitution with the chlorine in $[AuCl_4]^-$. This may be avoided by ether using TOABr and $[AuBr_4]^-$ or TOACl and $[AuCl_4]^-$.[11] The reduction of $[AuX_4]^-$ either to $[AuX_2]^-$ as in eq 1 or polymeric $[Au(I)SR]_n$ complex by addition of RSH are shown as process ii and iii, respectively. The formation of polymeric $[Au(I)SR]_n$ is concomitant with the distribution of H^+ and X^- from the organic to aqueous phase. Following the formation of Au(I), $NaBH_4$ is added to reduce the Au(I) intermediate(s) to metallic gold. This occurs either as a heterogeneous redox reaction between organic phase $[AuX_4]^-$, $[AuX_2]^-$, or polymeric $[Au(I)SR]_n$ complexes and aqueous phase $NaBH_4$ or as a homogeneous redox reaction in the organic phase between those ionic gold species and BH_4^-, which has transferred from the aqueous to the organic phase (process iv). To maintain the electroneutrality of both phases,

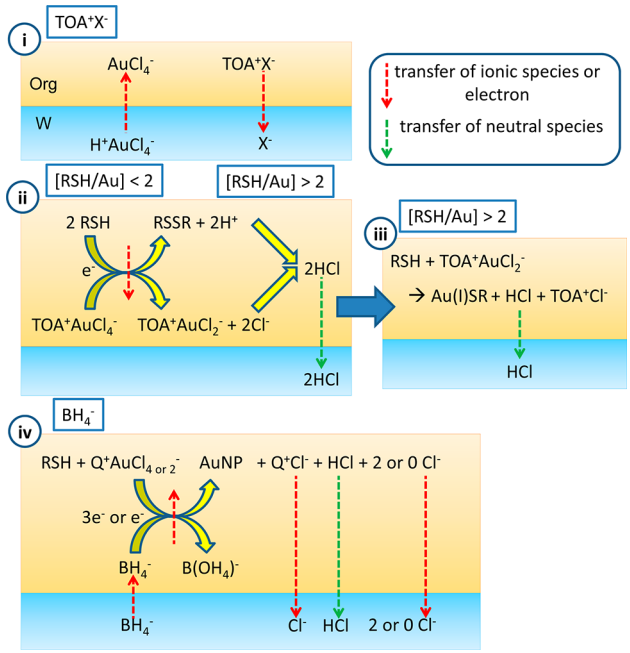

Figure 1. Brust−Schiffrin nanoparticle deposition processes: (i) ion exchange process, (ii, iii) reaction process between Au chloride ions and RSH, and (iv) reduction of Au chloride ions by BH_4^-.

Cl^- formed from Au chloro-complexes should transfer from the organic to aqueous phase as a common ion. Electrochemically controlled ion and electron transfer reactions have been used to probe metal deposition at the liquid−liquid interface.[20−28] Ion or electron transfer at the interface is observed at a potential that is dependent on the Gibbs energy of transfer of the ions or differences of redox potential between reductant and oxidant sequestered in either phase.[29] By measuring the redox potential of Au and appropriate reductants, as well as the Gibbs energy of ion transfer, effective metal deposition systems have been proposed.[30,31] For the specific case of Au distribution across the liquid−liquid interface, electrochemical ion transfer of $[AuCl_4]^-$[24,26,32,33] and $[AuCl_2]^-$[33] has been reported.

Key to a detailed understanding of the Brust−Schiffrin process is the ability to prove the oxidation state and coordination of the Au in the organic and aqueous phases. X-ray absorption fine structure (XAFS) is an ideal approach to obtain such information: numerous XAFS studies of the coordination structure of Au complexes have been carried out,[34−39] including the identification of valency in the reaction of Au and 1-dodecanethiol from the X-ray absorption near-edge structure (XANES) and the characterization of Au−Cl and Au−S bonds through the analysis of the extended X-ray absorption fine structure, EXAFS.[40−43]

In the present study, the Brust−Schiffrin nanoparticle preparation method is investigated by voltammetry for charge transfer at the interface between two immiscible electrolyte solutions (ITIES), XANES, and transmission electron microscopy (TEM). As metal precursors, $[AuCl_4]^-$ and $[AuCl_2]^-$ salts were used in the presence of RSH in 1,2-dichloroethane (DCE) and toluene (TL). To avoid the formation of mixed halide gold complexes, tetraoctylammonium chloride (TOA^+Cl^-) was used instead of TOA^+Br^-. We analyzed the processes proposed in Figure 1 by changing the holding time before the measurement and the concentration ratio of RSH/Au. Based on the ion transfer reaction obtained in the measurement, the effect of the

DOI: 10.1021/jacs.5b07825
J. Am. Chem. Soc. 2015, 137, 15135−15144

holding time and the RSH/Au concentration ratio on the nanoparticle formation by the reductant borohydride was also discussed, and important mechanistic insights were obtained.

RESULTS AND DISCUSSION

Ion Exchange Reaction of $[AuCl_4]^-$ from Water and the Cl^- of TOA^+Cl^- from DCE. $TOA^+[AuCl_4]^-$ in DCE has been prepared by a shake flask method using TOA^+Cl^- in DCE and $H^+[AuCl_4]^-$ in aqueous solution as in the Brust–Schiffrin method.[1] In order to understand process I (Figure 1), we measured the ion transfer of $[AuCl_4]^-$ from water to organic DCE at the micro-interface as shown in the voltammetric response (a) of Figure 2. For the case of the anions shown here,

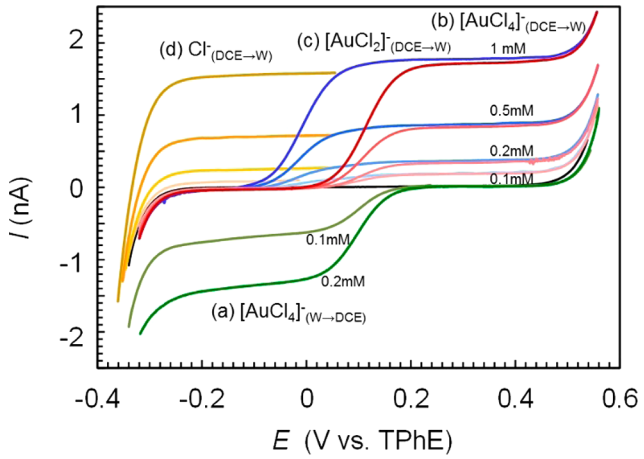

Figure 2. Voltammograms for the transfer of $[AuCl_4]^-$, $[AuCl_2]^-$, and Cl^- between water and DCE. Curves a, 0.1 and 0.2 mM $H^+[AuCl_4]^-$ in water; curves b, 0.1, 0.2, 0.5, and 1 mM $TOA^+[AuCl_4]^-$ in DCE; curves c, 0.1, 0.2, 0.5, and 1 mM $TOA^+[AuCl_2]^-$ in DCE; curves d, 0.1, 0.2, 0.5, and 1 mM TOA^+Cl^- in DCE. The potential scanning rate was 5 mV s^{-1}.

increasing potentials of transfer indicate increasing lipophilicity. The diffusion current was proportional to the concentration of $[AuCl_4]^-$ from 0.1 to 1 mM, indicating that the current was controlled by the diffusion of $[AuCl_4]^-$ in water. The half-wave potential for the transfer as shown in eq 2 was calculated to be 0.115 V.

$$[AuCl_4]^-_{(O)} \rightleftharpoons [AuCl_4]^-_{(W)} \quad (2)$$

An acidified aqueous phase (10 mM HCl) was used to avoid the partial hydrolysis of $[AuCl_4]^-$, which occurs in aqueous solutions at high pH.[44] The presence of $[Au(OH)Cl_3]^-$ and $[Au(OH)_2Cl_2]^-$ would affect the reduction by RSH and subsequent particle formation because of the different reduction potentials of the hydrolyzed complexes, which are relatively more hydrophilic. The transfer of $[AuCl_4]^-$ (dissolved in DCE as $TOA^+[AuCl_4]^-$) from DCE to water was observed as a positive current as shown in curves b of Figure 2. The transfer potential was identical to the transfer of $[AuCl_4]^-$ (dissolved as $HAuCl_4$) from water to DCE. Because these two species were indistinguishable, all subsequent experimental work utilized $TOA^+[AuCl_4]^-$, which is soluble in the organic phase, instead of repeating the phase transfer process.

When TOA^+Cl^- (the phase transfer catalyst in the Brust–Schiffrin reaction) was dissolved in DCE, the transfer of Cl^- from DCE to water was observed at the negative end of the potential window (transfer potential of −0.32 V) as shown in curve d in Figure 2 (eq 3):

$$Cl^-_{(O)} \rightleftharpoons Cl^-_{(W)} \quad (3)$$

In the preparation of $TOA^+[AuCl_4]^-$, the aforementioned ion exchange between Cl^- in organic and $[AuCl_4]^-$ in water (process i) proceeds spontaneously based on the Gibbs energies for the transfer of Cl^-[45,46] and $[AuCl_4]^-$[33] and their concentrations. Here, the phase boundary potential,[47] which is defined by the transfer of Cl^- present in excess as TOA^+Cl^- in the organic solution and $[AuCl_4]^-$ in water before equilibrium has been reached, determines the distribution of ionic species between water and the organic phase. The phase boundary potential is shifted to a negative potential due to the presence of organic phase TOA^+ and concentration of Cl^- in the two phases at equilibrium. This phase boundary potential prevents the loss of Au-containing ionic species into the aqueous phase because it is below that required for Au ion transfer. In the case of the TOA^+Br^-, which has also been used as a catalyst to transfer gold into the organic phase in the Brust–Schiffrin method, ion exchange proceeds as in process i though Br^- is rather hydrophobic.[45,46] By contrast, TOA^+ and H^+ do not transfer between water and DCE because of their respective hydrophobicity and hydrophilicity,[45] although a specific interaction between TOA^+ and $[AuCl_4]^-$ has recently been proposed.[48]

Chemical and Electrochemical Reaction between $[AuCl_4]^-$ and RSH: Time Dependence. The second step in the Brust–Schiffrin synthesis, the reaction between $TOA^+[AuCl_4]^-$ and RSH in DCE before the addition of BH_4^-, was studied using a macroscopic ITIES. Insoluble thiolate has been shown to form at the water–organic interface when the aqueous phase is retained during the thiol addition.[13] However, the extent of insoluble thiolate formation has not been quantified. Cyclic voltammograms were measured for the transfer of $[AuCl_4]^-$ between water and DCE containing 0.2 mM $TOA^+[AuCl_4]^-$ in the absence of RSH as shown in Figure 3A. Immediately after addition of 0.1 mM RSH (20 μL of 10 mM RSH) into 2 mL of DCE, the cyclic voltammogram was measured. The transfer current indicative of the concentration of $[AuCl_4]^-$ began to decrease after the RSH addition. Three hours later, a new pair of voltammetric peaks were observed at 0.002 and −0.065 V. The transfer potential in Figure 3A with a new peak at −0.005 V was identified as the transfer of $[AuCl_2]^-$[33] as per eq 4. For comparison, the transfer of $[AuCl_2]^-$ in the absence of thiol is included as a dotted line in Figure 3A.

$$[AuCl_2]^-_{(O)} \rightleftharpoons [AuCl_2]^-_{(W)} \quad (4)$$

The $[AuCl_2]^-$ peak current increased with time indicating the buildup of $[AuCl_2]^-$ until a near constant current was reached after 17 h. The decrease of the $[AuCl_4]^-$ peak mirrors the increase in the $[AuCl_2]^-$ peak indicating that $[AuCl_4]^-$ is being directly converted into $[AuCl_2]^-$. $[AuCl_2]^-$ was formed by the oxidation of RSH to RSSR disulfide in the DCE phase, consistent with the process described in eq 5[11] and process ii in Figure 1:

$$TOA^+[AuCl_4]^-_{(O)} + 2RSH_{(O)} \rightleftharpoons TOA^+[AuCl_2]^-_{(O)} + RSSR_{(O)} + 2HCl_{(W)} \quad (5)$$

DOI: 10.1021/jacs.5b07825
J. Am. Chem. Soc. 2015, 137, 15135–15144

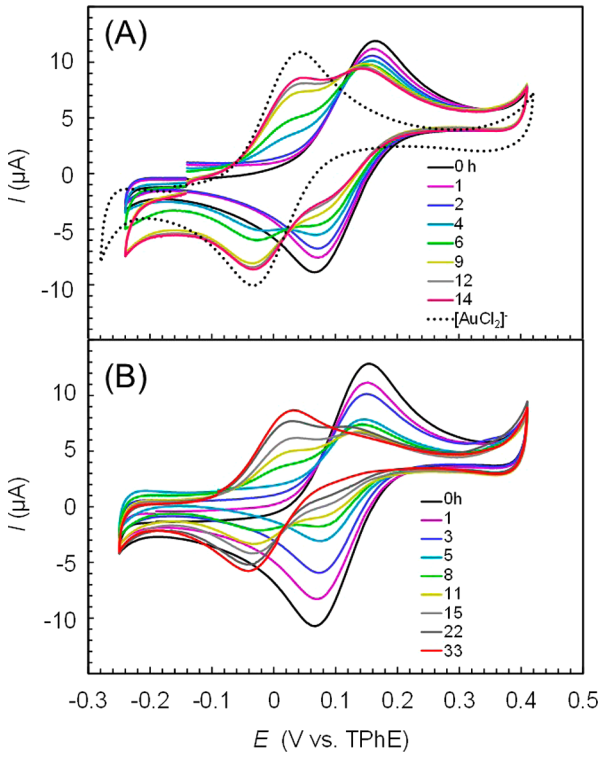

Figure 3. Time dependence on the reaction of $[AuCl_4]^-$ with RSH. Voltammogram at the macro-interface between 10 mM HCl in water and 0.2 mM $TOA^+[AuCl_4]^-$ with added (A) 0.1 mM RSH + 10 mM TOA^+TFPB^- and (B) 0.4 mM RSH + 10 mM TOA^+TFPB^-. Dotted line in panel A shows the transfer of $[AuCl_2]^-$ in the absence of thiol as a standard. The potential scan rate was 10 mV s^{-1}.

Here, the HCl byproduct transfers from DCE to water; the dissociation constant of the acid in the organic phase can explain the lack of observed ion transfer current. We note that Duong et al. have also studied this process using octanethiol as the reducing agent.[48] They saw only a small change in the $[AuCl_4]^-$ transfer current, although the thiol was added to the aqueous phase and the time-scale of the reaction with thiol was not clear.

When the concentration of RSH is higher than that of $[AuCl_4]^-$, that is, 0.4 mM RSH and 0.2 mM $[AuCl_4]^-$, the time dependent $[AuCl_4]^-$ voltammetry evolved distinctly from the case of lower RSH concentration described above (0.1 mM RSH). Voltammograms were measured from 0 to 33 h after RSH addition to DCE as shown in Figure 3B. Though the transfer current of $[AuCl_4]^-$ decreased over a period from 0.5 to 6 h, the transfer current of the $[AuCl_2]^-$ reduction product, indicated above, was not observed here. Unlike Figure 3A where a symmetrical voltammogram resulted from the interconversion of species, the transfer current due to $[AuCl_2]^-$ following eq 5 was only seen after 6 h. These results show that about 50% of the total concentration of Au did not form $[AuCl_2]^-$, but another product resulted, which was not observed in the voltammogram at the macro-interface. The concentration dependence observed above is investigated in the next section to confirm the identity of the new species and quantify the role of RSH.

Chemical and Electrochemical Reaction between $[AuCl_4]^-$ and RSH: Concentration Dependence of RSH. The voltammogram was recorded at the micro-interface between water, containing 10 mM HCl as supporting electrolyte, and the DCE containing various concentration ratios of Au and RSH (ratio of RSH/$[AuCl_4]^-$ r = 0, 0.4, 1, 2, 3, 4, and 8). The voltammograms were measured over a period of 5 days (Figure 4A–D). Here, the initial $[AuCl_4]^-$ concentration

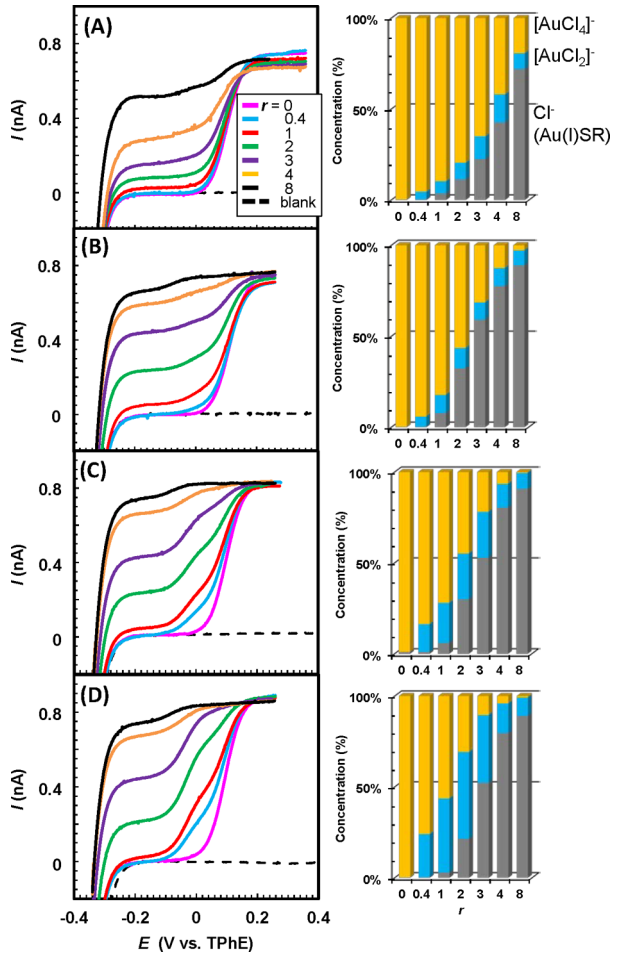

Figure 4. Effect of reaction time and RSH concentration on the reaction of $[AuCl_4]^-$ with RSH. (left) Voltammograms at the micro-interface between 10 mM HCl in water and DCE solutions containing 0.5 mM $TOA^+[AuCl_4]^-$, 0, 0.2, 0.5, 1, 1.5, 2, or 4 mM RSH (corresponding to r = 0, 0.4, 1, 2, 3, 4, or 8), and 1 mM TOA^+TFPB^-. Voltammograms were measured directly after preparation and 1, 2, and 5 days later (A, B, C, and D). The scan rate was 5 mV s^{-1}. (right) The concentrations of $[AuCl_4]^-$, $[AuCl_2]^-$, and Au(I)SR were determined from the diffusion current of each species.

was 0.5 mM. The measurements were performed at different time periods: right after the preparation of the solutions and after 1, 2, and 5 days.

As observed previously,[13] a white precipitate rapidly accumulated at the interface between water and DCE when $r \geq 2$. The presence of the precipitate blocks the interface, reducing the ion transfer currents.[49] To avoid this phenomenon, the pellucid DCE phase of each sample was separated from the precipitate and contacted with a fresh aqueous solution for further voltammetry. This is not a major concern during the duration of the experiment because the small interfacial contact area means that the system is effectively a single-phase reaction. As shown in Figure 4, three positive currents were observed; the first positive current occurs at −0.18 V, the second current at −0.01 V is assigned to the $[AuCl_2]^-$ transfer, and the third

DOI: 10.1021/jacs.5b07825
J. Am. Chem. Soc. 2015, 137, 15135–15144

current at 0.11 V is assigned to the $[AuCl_4]^-$ transfer. The −0.18 V transfer, which was not clearly observed at the macro-interface (Figure 3), corresponds to the transfer of a more hydrophilic anion from DCE to water or alternatively a hydrophobic cation from water to DCE. It is suggested that the current corresponds to the transfer of Cl^- dissociated from $[AuCl_2]^-$ during the formation of $[Au(I)SR]_n$ in DCE as in process iii in Figure 1. This is because the ion transfer potential occurs at a similar potential to those observed in curve d of Figure 2, which correspond to the transfer of Cl^- from TOA^+Cl^-. The proposed chemical reaction between $TOA^+[AuCl_2]^-$ and RSH is given in eq 6:

$$TOA^+[AuCl_2]^-_{(O)} + RSH_{(O)} \rightleftharpoons Au(I)SR_{(O)} + TOA^+Cl^-_{(O)} + HCl_{(W)} \quad (6)$$

Here, transfer of Cl^- formed from TOA^+Cl^- in DCE was observed in the voltammogram as curve d in Figure 2. In the reduction of $[AuCl_4]^-$ to $[AuCl_2]^-$, the Cl^- from $[AuCl_4]^-$ is generated in conjunction with H^+ as two RSH form RSSR and two H^+ (eq 1)[11] facilitating the formation of HCl as a hydrophilic neutral species (Figure 1, process ii). As a result, the concentration of Cl^- transferred is identical to the concentration of Au(I)SR formed in DCE. Here, soluble Au(I)SR may form the polymeric species, $[Au(I)SR]_n$, which is visible as a white precipitate. Though it has been reported that the solubility of Au(I)SR is very low,[11] Cl^- transfer was also observed in the absence of a visible white precipitate $[Au(I)SR]_n$. Because TOA^+Cl^- remains soluble during the reaction, an accurate concentration of Au(I)SR may be measured indirectly from the Cl^- concentration after the removal of the white precipitate. The concentration ratios of $[AuCl_4]^-$, $[AuCl_2]^-$, and Cl^- calculated from the limiting currents were plotted as a function of r and time in Figure 4 (right). Here, the current corresponding to $[AuCl_2]^-$ transfer was calculated by the subtraction from the current corresponding to $[AuCl_4]^-$ as shown in Figure S1. On the basis of the measurements at the micro-interface, it can be seen that the concentration ratio of $[AuCl_4]^-$, $[AuCl_2]^-$, and Cl^- (indirectly, Au(I)SR) were dependent on time as well as thiol to gold ratio. The concentration of $[AuCl_2]^-$ slowly increased depending on the duration of the contact time for $0.4 \leq r \leq 3$. We note that the $[AuCl_2]^-$ concentration was highest at $r = 2$; beyond this ratio the $[AuCl_2]^-$ concentration falls. The $[AuCl_2]^-$ concentration was less than 10% of the total gold immediately after the sample preparation, independent of r, while Cl^- transfer (related to Au(I)SR) was observed to be more than 70% at $r = 8$ (Figure 4). The concentration of Au(I)SR formed in DCE increased with the amount of thiol added. It should be noted that approximately 20% of the Au was present as Au(I)SR when $r = 2$, whereas previously it has been reported that Au(I)SR was not formed alongside $[AuCl_2]^-$ at $r = 2$, when the aqueous phase was removed.[11] These results obtained on the time dependence of the reaction indicate that Au(I)SR could form directly from $[AuCl_4]^-$ at $r > 2$ because Au(I)SR formation was quicker than $[AuCl_2]^-$ formation as in eq 7, as opposed to the two-step reaction in eqs 5 and 6 and Figure 1, process i and ii.

$$TOA^+[AuCl_4]^-_{(O)} + 3RSH_{(O)} \rightleftharpoons Au(I)SR_{(O)} + RSSR_{(O)} + TOA^+Cl^-_{(O)} + 3HCl_{(W)} \quad (7)$$

This process was also supported by the results obtained at the macro-interface (Figure 3B) where a delay is noted between the onset of $[AuCl_4]^-$ reduction and $[AuCl_2]^-$ evolution. As stated previously, the Cl^- transfer indicative of Au(I)SR formation could not be detected in the macro-interfacial set up.

XAFS measurements were taken of a solution containing 5 mM $TOA^+[AuCl_4]^-$ and various equivalents of RSH in TL. At a low thiol concentration ($r = 0.5$), the solution was examined over a number of hours. It was found that there was a clear time dependence to the reaction over a time scale longer than that typically utilized in the Brust−Schiffrin synthesis, Figure 5A. To

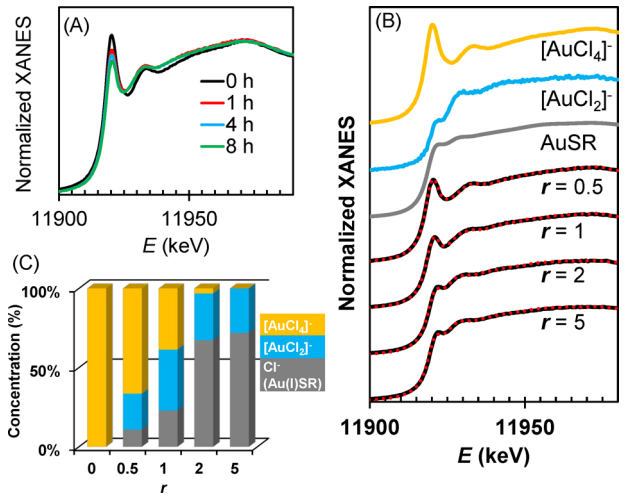

Figure 5. (A) Time dependence of the reaction at RSH/Au ratio $r = 0.5$ showing the variation in spectra on increased reaction time. (B) Linear combination fitting (LCF) of the XANES data collected for the addition of thiol to $AuCl_4$ in toluene: solid line, experimental data; dotted line, fit to standards. Normalized data sets and LCF fit for $r = 0.5$, 1, 2, and 5. The standard spectra used for the fitting were $TOA^+[AuCl_4]^-$, $TBA^+[AuCl_2]^-$, and $[Au(I)SR]_n$. (C) Concentrations of $[AuCl_4]^-$, $[AuCl_2]^-$, and Au(I)SR were derived from the LCF.

enhance the reaction, samples were scanned with stirring at times >10 h after mixing. Figure 5B shows the XAFS results at $r = 0.5$, 1, 2, and 5 and the linear combination fitting to pure standard spectra for $TOA^+[AuCl_4]^-$, $TBA^+[AuCl_2]^-$, and $[Au(I)SR]_n$. These standards are also plotted for comparison. A solution of $TOA^+[AuCl_4]^-$ was used for Au(III), $[AuCl_2]^-$ was extracted from a solution of $TBA^+[AuCl_2]^-$ as detailed previously,[39] and a solid spectrum of dried $[Au(I)SR]_n$ precipitate was used to examine the possible presence of gold thiolate. Principal component analysis was performed on the data set indicating that there were three different gold species present in the system (Figure S3 and S4). The results on increasing thiol concentration clearly demonstrate an increase in the extent of reduction. As can be seen in Figure 5C, $[Au(I)SR]_n$ is present as a component of the best fit at all thiol concentrations suggesting its formation as a minor component even below the stoichiometric ratio required for complete reduction. The initial increase in $[AuCl_2]^-$ content, which then decreases, suggests that the thiol may replace Cl as a ligand for Au(I). Figure 5C shows a similar ratio of products to those determined electrochemically in Figure 4D, the samples measured at the micro-interface after 5days.

Chemical Reaction between $[AuCl_2]^-$ and RSH. The behavior of $[AuCl_2]^-$ and RSH was also studied to see whether any further reactions occur following the formation of $[AuCl_2]^-$

DOI: 10.1021/jacs.5b07825
J. Am. Chem. Soc. 2015, 137, 15135−15144

by RSH. The same experimental procedure as the previous section of $[AuCl_4]^-$ experiments was used; however, this time $TOA^+[AuCl_2]^-$ was used instead of $TOA^+[AuCl_4]^-$ as a source of Au(I). An initial concentration of 0.5 mM $TOA^+[AuCl_2]^-$ was dissolved in DCE alongside 1-dodecanethiol where r = 0, 0.2, 0.4, 1, 2, and 4. The voltammograms obtained are shown in Figure 6. The $[AuCl_2]^-$ transfer current decreased with

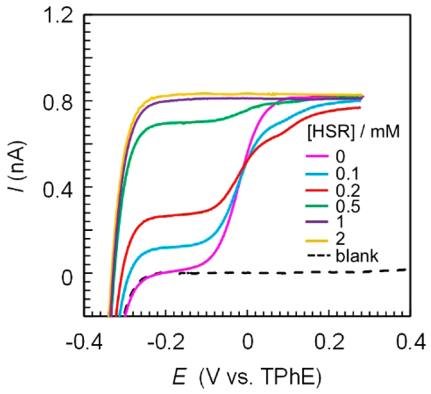

Figure 6. RSH concentration dependence on the reaction of $[AuCl_2]^-$ with RSH. Voltammograms at the micro-interface between 10 mM HCl in water and 0.5 mM $TOA^+[AuCl_2]^-$ with 0, 0.1, 0.2, 0.5, 1, and 2 mM RSH and 1 mM TOA^+TFPB^-. Voltammograms were measured 1 day after mixing. The scan rate was 5 mV s^{-1}.

increasing RSH concentration. Also, the transfer of Cl^- corresponding to the formation of Au(I)SR was observed. At RSH = 1 mM, it was found that about 90% of the $[AuCl_2]^-$ species had reacted to form Au(I)SR, indicating that $[AuCl_2]^-$ reacted stoichiometrically with RSH to form Au(I)SR verifying the reaction given in eq 6. On the other hand, when the $[AuCl_2]^-$ concentration was higher than RSH, that is, [RSH] = 0.1 and 0.2 mM, $[AuCl_4]^-$ was formed as 10% of the total Au concentration through the disproportionation of Au^+, which was an intermediate species between $[AuCl_2]^-$ and Au(I)SR and very unstable.

Deposition Mechanism on the Reduction of Au Chloride Ions by BH_4^-. The mechanism for the formation of gold nanoparticles in the presence of BH_4^- was investigated to examine the reaction process as shown in Figure 1, process iv. Reaction iv involves reduction within the DCE bulk phase following BH_4^- transfer from water to DCE. However, alternative processes involving heterogeneous redox reactions are possible whereby $[AuCl_4]^-$, $[AuCl_2]^-$, or Au(I)SR present in the organic phase are reduced at the interface by aqueous phase BH_4^-. In order to distinguish between ion and electron transfer reactions, as well as to avoid ion transfers that are not involved in the redox reaction between Au ions and BH_4^-, voltammetric measurements were performed in a bipolar cell. In this cell, the aqueous and organic phases were not in direct contact but were connected by a solid electrode.[50] Therefore, electron transfer may be examined in the absence of any ion transfer reactions. Here, glassy carbon and platinum wire electrodes were used in water and DCE, respectively, to connect the two phases. However, no current corresponding to the electron transfer between water and DCE was observed. We therefore suggest that the ion transfer of BH_4^- from water to DCE must occur prior to homogeneous reduction of Au chloride ions within the DCE phase, Figure 1, process iv. Voltammograms were also recorded directly at the interface between water containing BH_4^- and DCE in the absence of Au chloride ions and RSH. An ion transfer current was observed at −0.3 V; the current was seen to increase with the concentration of BH_4^- as shown in Figure 7 and described in eq 8:

$$BH_4^-{}_{(W)} \rightleftharpoons BH_4^-{}_{(O)} \quad (8)$$

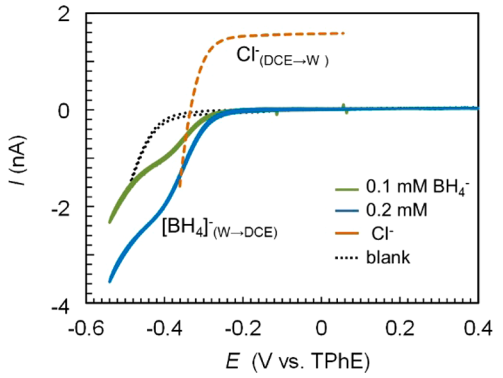

Figure 7. Voltammograms for the transfer of BH_4^- between water and DCE. Solid lines are 0, 0.1, 0.2, 0.4, and 0.6 mM $NaBH_4$ and 1 mM LiOH in water. The dotted line shows the voltammogram for the transfer of Cl^- (1 mM TOA^+Cl^- in DCE, curve c in Figure 2). The scan rate was 5 mV s^{-1}.

The half wave potential for the transfer of BH_4^- was calculated to be −0.36 V. Here, 1 mM LiOH was employed as a supporting electrolyte in order to avoid the decomposition of BH_4^-. This result suggests that the BH_4^- reaction with Au ions is not an interfacial one but occurs in the organic phase after the transfer from water to the organic phase (process iv). Although the BH_4^- ion transfer occurs at quite a negative potential because of its hydrophilicity, in the standard chemical Brust−Schiffrin process, the phase transfer may also be driven by Cl^- transfer from TOA^+Cl^-, which is added in a large excess to enable the initial transfer of $[AuCl_4]^-$ from the aqueous phase to the organic.[15] The transfer of BH_4^- from water to DCE overlaps with that of Cl^- (dotted line in Figure 7) resulting in the phase transfer reaction of BH_4^- and Cl^-. The phase boundary potential is negative of the Au ion transfer potential as defined by the presence of very hydrophilic ions (Cl^-) preventing the transfer of Au-containing ionic species into the aqueous phase.Therefore, the Au ion reduction occurs in the organic phase following BH_4^- transfer from water as in eq 9:

$$TOA^+[AuCl_2]^-{}_{(O)} + BH_4^-{}_{(O)} \rightleftharpoons Au_{(O)} + TOA^+Cl^-{}_{(O)} + HCl_{(W)} + B(OH)_4^-{}_{(W)} \quad (9)$$

$[AuCl_4]^-$ may also be reduced by BH_4^- without the initial reduction by RSH.[16] The decomposition products of BH_4^-, for example, to $B(OH)_4^-$, have not been confirmed, therefore we have not conserved the electroneutrality of eq 9.

Effect of Time and Concentration Ratio on NP Formation. In order to confirm the reactivity of $[AuCl_4]^-$, $[AuCl_2]^-$, and Au(I)SR with $NaBH_4$, 1 mM $NaBH_4$ was added to gold thiol mixtures at a number of RSH/Au ratios, either right after sample preparation (series A) or 5 days after mixing (series B). Following the immediate addition (series A), when RSH was absent, metallic gold was formed instantly in both the

DOI: 10.1021/jacs.5b07825
J. Am. Chem. Soc. 2015, 137, 15135−15144

water and DCE phases. At 0.2 mM RSH (r = 0.4), the solution turned a pink color, whereas a brown solution developed when 0.5−4 mM RSH (r = 1−8) was added to the sample, which relates to the size of the particles formed. A clear absorption peak was not always observed in UV−vis absorption spectroscopy (Figure S2A) TEM measurements were also performed to determine the dependence of particle size on reaction conditions as shown in series A and B of Figure 8. The average particle diameter was 1.8 nm at r = 0.4, and the size slightly decreased from 1.5 to 1.0 nm for $r \geq 1$, which agrees with the variation seen in the literature in toluene systems as compiled by Perala and Kumar.[15] The concentration of nanoparticles formed from solutions that were allowed to stand for 5 days was higher than that for solutions reduced initially at r = 1−3 based on the change in absorbance of the UV−vis spectra (Figure S2A,B). Although the spectroscopic data indicated that particle sizes were slightly larger than those obtained from the fresh samples, the electron microscopy suggested that the size distributions of the two sets of particles were similar. On the other hand, at a higher thiol concentration (r = 4 and 8) the number of particles fell progressively in the aged sample (Figure S2B), in marked contrast to the fresh samples at r = 4 and 8. On aging of the reaction mixture, an increase in particle size was seen from 1.8 to 2.5 nm at r = 0.4. This is because RSH was consumed for the reduction of $[AuCl_4]^-$ as in eq 5. The RSH concentration at r = 0.4 in 5 days was calculated to be negligibly small (<0.05 mM) based on the $[AuCl_2]^-$ concentration in Figure 4D. Particle size was critically dependent on the RSH concentration at r = 0.4. There was less variation in particle size, between 1.0 and 1.5 nm, at r = 1 or r = 2. Whereas formation of $[AuCl_2]^-$ by RSH seems to produce a higher nanoparticle concentration, a strong dependence of particle size on the relative concentrations of $[AuCl_4]^-$ and $[AuCl_2]^-$ was not observed in this study. Here, the RSH concentrations remaining after 5 days were calculated to be 0.2 and 0.3 mM at r = 1 and r = 2, respectively, based on the concentrations of $[AuCl_2]^-$ and Au(I)SR. As a result, particle sizes from 1.0 to 1.5 nm were obtained independently of the time allowed for sample preparation. Above r = 2, there is little nanoparticle formation in the aged sample, suggesting that the insoluble, polymeric $[Au(I)SR]_n$ species is not readily reduced by sodium borohydride.[18] Time dependent size evolution has previously been observed following $NaBH_4$ addition,[51] but this is the first demonstration that the product size depends on the $[AuCl_4]^-$ and RSH mixing time.

CONCLUSIONS

The mechanistic details of the Brust−Schiffrin nanoparticle synthesis were investigated by voltammetry, XAFS, and TEM. Ion transfers related to the formation mechanism such as $[AuCl_4]^-$, $[AuCl_2]^-$, Cl^- (Au(I)SR), and BH_4^- were measured at a water/DCE interface. $TOA^+[AuCl_4]^-$ was prepared by ion exchange reaction between $[AuCl_4]^-$ in water and Cl^- in DCE (Figure 1, process i). $[AuCl_2]^-$ was formed from the reduction of $[AuCl_4]^-$ by RSH (Figure 1, process ii). When the thiol concentration exceeded that required for the stoichiometric reaction, TOA^+Cl^-, HCl, and a white precipitate were also formed (Figure 1, process iii). It was found that $[AuCl_2]^-$ was formed under the concentration ratio of RSH/Au $0.2 \leq r \leq 2$, and the increase in concentration was time-dependent over a period of 5 days. On the other hand, $[AuCl_2]^-$ concentration decreased at $r > 2$ after 24 h because of Au(I)SR formation. The concentration ratios of $[AuCl_4]^-$, $[AuCl_2]^-$, and Au(I)SR

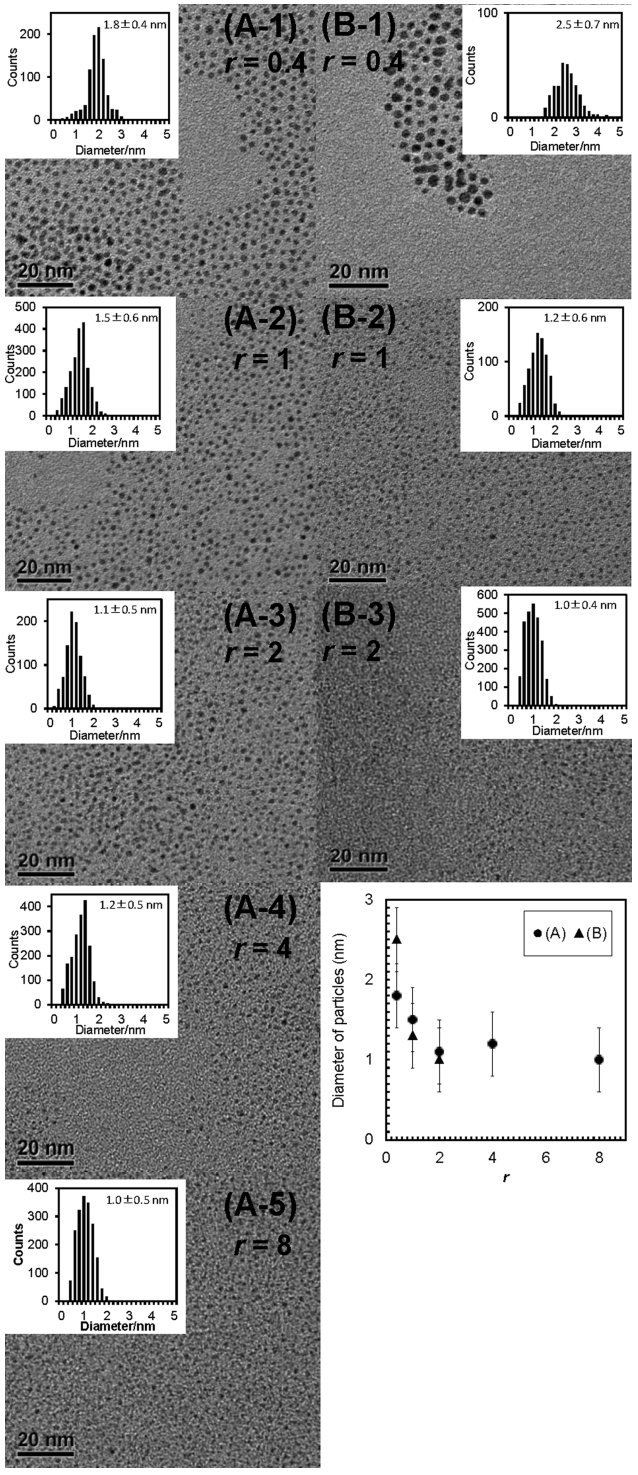

Figure 8. TEM images and size distribution after the reduction by BH_4^-. Series A are samples prepared by BH_4^- addition right after mixing of $[AuCl_4]^-$ and RSH (r = 0.4−8). Series B are samples prepared by BH_4^- addition 5 days after mixing of $[AuCl_4]^-$ and RSH (r = 0.4−2). Particle size distributions are included next to each image. The bottom right figure shows the relationship between average particle diameter and concentration ratio of RSH/Au concentration ratio.

based on ion transfer currents at the ITIES were consistent with those based on XANES analysis of the corresponding homogeneous reaction. In the presence of the borohydride ion, BH_4^-, in water, the redox reaction between $[AuCl_4]^-$ or

DOI: 10.1021/jacs.5b07825
J. Am. Chem. Soc. 2015, 137, 15135−15144

$[AuCl_2]^-$ and BH_4^- proceeds in DCE, following BH_4^- transfer from the aqueous phase. Cl^-, formed by the dissociation of $[AuCl_2]^-$, transferred from DCE to water to maintain electroneutrality between the two phases (Figure 1, process iv). The insoluble form of the $[Au(I)SR]_n$ species was not reduced by BH_4^- to form nanoparticles. As can be seen from the electrochemical observations, despite the use of a liquid/liquid system in the Brust–Schiffrin synthesis, all of the reduction reactions occur within the organic phase with the aqueous phase only acting as a source for $[AuCl_4]^-$ and BH_4^-. The volume and size of nanoparticles formed depended on the thiol to gold ratio as well as the mixing duration because of the $[Au(I)SR]_n$ formation. Higher concentrations of nanoparticles of 1.0–1.5 nm diameter were formed for $1 \leq r \leq 2$.

EXPERIMENTAL SECTION

Chemicals. Hydrogen tetrachloroaurate, $HAuCl_4\ 3H_2O$ (Alfa, ≥99.999%), was used as the source of Au(III); tetrabutylammonium dichloroaurate, $TBA^+[AuCl_2]^-$ (Tokyo Kasei, ≥ 99.99%) was used as the Au(I) source. HCl was used as a supporting electrolyte (WAKO Co. Ltd.) to avoid the hydrolysis of the Au–chloro complex.[44] 1,2-Dichloroethane, DCE (≥99%, Aldrich), and toluene, TL (≥99.8%, Aldrich), were used as the organic solvents: these were shaken twice with deionized water because it has been reported that large quantities of water could accelerate the formation of white precipitate, which was believed to be the oligomeric Au(I) thiolate species.[11] However, the organic solutions used for electrochemistry were saturated with water because gold nanoparticles have previously been prepared using two phases in the Brust–Schiffrin method[1] and the stirring required would lead to the saturation of the organic phase with water. 1-Dodecanethiol (RSH, ≥ 98%, Sigma-Aldrich) was used as the initial reductant. Tetraoctylammonium chloride, TOA^+Cl^- (97% Sigma-Aldrich), was used to generate gold salts that are stable in the organic phase. The TOA^+ salt of $[AuCl_4]^-$ was obtained as a precipitate through mixing of methanol solutions of TOA^+Cl^- and $HAuCl_4$ and was purified by recrystallization in ethanol.[11] The TOA^+ salt of $[AuCl_2]^-$ in DCE was prepared by shaking pure water with equimolar amounts of $TBA^+[AuCl_2]^-$ and TOA^+Cl^- in DCE. The supporting electrolyte in DCE for potential sweep experiments was TOA^+TFPB^- or $BTPPA^+TFPB^-$, where $BTPPA^+$ and $TFPB^-$ denote bis-(triphenylphosphoranylidene) ammonium cation and tetrakis[3,5-bis(trifluoromethyl)phenyl] borate anion, respectively. $BTPPA^+TFPB^-$ was obtained by metathesis of $BTPPA^+Cl^-$ and Na^+TFPB^-.[52] Equimolar quantities of the two reactants were dissolved separately in methanol and then mixed and stirred for ∼1 min. The mixture was allowed to stand for 30 min before filtering under atmospheric conditions. The dried product was then recrystallized in ethanol.

Measurement of the Voltammogram for Charge Transfer at the Macro- and Micro-Water/DCE Interfaces. Two electrochemical cells were employed; a macro-interface cell and a micro-interface cell. Cyclic voltammetry experiments were performed using a four electrode configuration with an IVIUM potentiostat ("Compactstat" model, IVIUM Technologies, The Netherlands). No *iR* compensation was applied for the electrochemical measurements. In the (conventional) macro-interface cell, homemade Ag/AgCl and platinum gauze were used as reference (RE) and counter (CE) electrodes, respectively. The organic CE was insulated from the aqueous phase by coating its contact in a glass sheath. The cell used for the electrochemical measurements at the water/DCE interface had a cross-sectional area of about 0.64 cm^2 and a volume of 3 cm^3. Further details are described elsewhere.[26] The micro-interface cell uses a 16 μm thick polyester film with a microhole of 30 μm in diameter to separate the water and DCE phases.[53−55] The potential difference at the water/DCE interface, E, was measured as a function of the potential of a Ag/AgCl electrode in water. For the RE in DCE, the potential is referred to that of a $BTPPA^+$ ion selective electrode, inserted in DCE. The generic cell composition is Ag|AgCl|10 mM LiCl (W)|W1 (W)||DCE1 (DCE)|10 mM $BTPPA^+TFPB^-$ (DCE)|1 mM $BTPPA^+Cl^-$ + 10 mM LiCl (W)|AgCl|Ag

E is related to the Galvani potential difference, $\Delta^{W}_{DCE}\phi$, as shown in eq 10.

$$E = \Delta^{W}_{DCE}\phi + E_{ref} \quad (10)$$

where E_{ref} is the potential of the reference electrodes employed. In the calculation of $\Delta^{W}_{DCE}G^\circ$ ($= -zF\Delta^{W}_{DCE}\phi^\circ$) the measured E was converted using the extrathermodynamic assumption of Parker.[56]

XANES Measurements and Analyses. XAFS spectra were acquired at the spectroscopy beamline I18 at the Diamond Light Source (Harwell Science and Innovation Campus, UK). Data were acquired in fluorescence-yield mode unless otherwise stated. The intensity of the Au L_3-fluorescence emission was monitored using an Ortec multielement solid state Ge detector.[57] 1-Dodecanethiol was added at RSH/Au ratios of r = 0.5, 1, 2, and 5 to solutions of $TOA^+[AuCl_4]^-$ (5 mM) in TL. The solutions were mixed and allowed to stand for >10 h before transferring to 2 mL Eppendorf tubes for XAFS measurements. $TOA^+[AuCl_4]^-$ was prepared as a standard for Au(III); the $[AuCl_2]^-$ standard spectrum was generated from a series of $TBA^+[AuCl_2]^-$ spectra as discussed previously.[39] The $[Au(I)SR]_n$ standard spectrum was collected at beamline B18 at the Diamond Light Source in transmission mode.[58] To produce the "white precipitate" $TOA^+[AuCl_4]^-$ (4.38 mM) was mixed in a 1:5 ratio with RSH (21.9 mM) in TL. The sample was mixed thoroughly and allowed to stand for 2 h. A 10-fold excess of methanol was then added causing a white precipitate to crash out of solution. After standing for 1 h, the mixture was centrifuged, and the powder was collected. The powder was washed with toluene and methanol and centrifuged a second time before drying. To collect the spectrum, 10 mg of the white precipitate was mixed with methyl cellulose and compressed into an 8 mm pellet. Elemental analysis confirmed that there was no halide content in the white precipitate formed. The XAFS spectra were analyzed by using the Athena package.[59] Samples were calibrated to gold foil samples collected at the beamtime and normalized to an edge height of 1. The normalized and calibrated spectra were then used to perform linear combination fitting in Athena. The strong XANES resonance visible in the spectra at the 11 918 eV region reflects an intra-atomic electronic transition of Au 2p core electrons to unoccupied valence states with d-characters. This produced a high intensity "white line" for Au(III) due to the high 6s and 5d orbital vacancies and the lower number of vacancies in Au(I) species results in a much lower peak at the absorption edge.[39] The high sensitivity to unoccupied valence d-states of Au allows the identification of Au oxidation state and ligands.

Nanoparticle Preparation and TEM Measurement. In order to examine the time dependence on the synthesized nanoparticles, TEM images of the fresh and aged sample solutions were taken. Nanoparticles were prepared by mixing $TOA^+[AuCl_4]^-$ and RSH in DCE, then either immediately or after leaving to stand for 5 days the DCE solutions were shaken with water containing $NaBH_4$ and 1 mM NaOH, to stabilize the borohydride solution. The DCE was then separated from the water phase and stored in a glass vial. Immediately prior to transmission electron microscopy, TEM (JEM-2100, JEOL), the nanoparticle solution was dropped on to the TEM grid (holey carbon films on 300 mesh copper grids, Agar Scientific) to isolate the deposit. Particle diameters were calculated using the ImageJ software.[60]

ASSOCIATED CONTENT

Supporting Information

The Supporting Information is available free of charge on the ACS Publications website at DOI: 10.1021/jacs.5b07825.

Cyclic volammogram analyses, UV–vis absorption spectra and principal component analysis on XANES spectra (PDF)

DOI: 10.1021/jacs.5b07825
J. Am. Chem. Soc. 2015, 137, 15135−15144

AUTHOR INFORMATION

Corresponding Author

*auehara@rri.kyoto-u.ac.jp

Notes

The authors declare no competing financial interest.

ACKNOWLEDGMENTS

This research was partly supported by The Kyoto University Foundation, Japan, and by Grants-in-Aid for Scientific Research (No. 25420905) from the Ministry of Education, Culture, Sports, Science and Technology, Japan. We thank Diamond Light Source Ltd for the provision of synchrotron beamtime (awards SP-8861 and SP-11293). R.A.W.D. and S.L.M.S. gratefully acknowledge financial support from the EPSRC through an EPSRC-NSF "Materials World Network" grant (EP/H047786/1). S.Y.C. gratefully acknowledges the award of a President PhD Scholarship by the University of Manchester.

REFERENCES

(1) Brust, M.; Walker, M.; Bethell, D.; Schiffrin, D. J.; Whyman, R. *J. Chem. Soc., Chem. Commun.* **1994**, 801.

(2) Leff, D. V.; Ohara, P. C.; Heath, J. R.; Gelbart, W. M. *J. Phys. Chem.* **1995**, *99*, 7036.

(3) Hostetler, M. J.; Wingate, J. E.; Zhong, C. J.; Harris, J. E.; Vachet, R. W.; Clark, M. R.; Londono, J. D.; Green, S. J.; Stokes, J. J.; Wignall.; et al. *Langmuir* **1998**, *14*, 17.

(4) Shon, Y. S.; Mazzitelli, C.; Murray, R. W. *Langmuir* **2001**, *17*, 7735.

(5) Liu, X.; Worden, J. G.; Huo, Q.; Brennan, J. R. *J. Nanosci. Nanotechnol.* **2006**, *6*, 1054.

(6) Shimmin, R. G.; Schoch, A. B.; Braun, P. V. *Langmuir* **2004**, *20*, 5613.

(7) Chen, S. W.; Templeton, A. C.; Murray, R. W. *Langmuir* **2000**, *16*, 3543.

(8) Corbierre, M. K.; Lennox, R. B. *Chem. Mater.* **2005**, *17*, 5691.

(9) Schaaff, T. G.; Shafigullin, M. N.; Khoury, J. T.; Vezmar, I.; Whetten, R. L.; Cullen, W. G.; First, P. N.; GutierrezWing, C.; Ascensio, J.; JoseYacaman, M. J. *J. Phys. Chem. B* **1997**, *101*, 7885.

(10) Alvarez, M. M.; Khoury, J. T.; Schaaff, T. G.; Shafigullin, M.; Vezmar, I.; Whetten, R. L. *Chem. Phys. Lett.* **1997**, *266*, 91.

(11) Goulet, P. J. G.; Lennox, R. B. *J. Am. Chem. Soc.* **2010**, *132*, 9582.

(12) Barngrover, B. M.; Aikens, C. M. *J. Am. Chem. Soc.* **2012**, *134*, 12590.

(13) Li, Y.; Zaluzhna, O.; Tong, Y. Y. J. *Langmuir* **2011**, *27*, 7366.

(14) Li, Y.; Zaluzhna, O.; Tong, Y. Y. J. *Chem. Commun.* **2011**, *47*, 6033.

(15) Perala, S. R. K.; Kumar, S. *Langmuir* **2013**, *29*, 9863.

(16) Li, Y.; Zaluzhna, O.; Xu, B. L.; Gao, Y. A.; Modest, J. M.; Tong, Y. J. *J. Am. Chem. Soc.* **2011**, *133*, 2092.

(17) Perala, S. R. K.; Kumar, S. *Langmuir* **2013**, *29*, 14756.

(18) Zhu, L. L.; Zhang, C.; Guo, C. C.; Wang, X. L.; Sun, P. C.; Zhou, D. S.; Chen, W.; Xue, G. *J. Phys. Chem. C* **2013**, *117*, 11399.

(19) Yu, C. H.; Zhu, L. L.; Zhang, R. C.; Wang, X. L.; Guo, C. C.; Sun, P. C.; Xue, G. *J. Phys. Chem. C* **2014**, *118*, 10434.

(20) Johans, C.; Lahtinen, R.; Kontturi, K.; Schiffrin, D. J. *J. Electroanal. Chem.* **2000**, *488*, 99.

(21) Johans, C.; Clohessy, J.; Fantini, S.; Kontturi, K.; Cunnane, V. J. *Electrochem. Commun.* **2002**, *4*, 227.

(22) Guo, J. *Electrochem. Commun.* **2003**, *5*, 1005.

(23) Trojanek, A.; Langmaier, J.; Samec, Z. *J. Electroanal. Chem.* **2007**, *599*, 160.

(24) Lepkova, K.; Clohessy, J.; Cunnane, V. J. *Electrochim. Acta* **2008**, *53*, 6273.

(25) Li, Q.; Xie, S. B.; Liang, Z. W.; Meng, X.; Liu, S. J.; Girault, H. H.; Shao, Y. H. *Angew. Chem., Int. Ed.* **2009**, *48*, 8010.

(26) Gründer, Y.; Ho, H. L. T.; Mosselmans, J. F. W.; Schroeder, S. L. M.; Dryfe, R. A. W. *Phys. Chem. Chem. Phys.* **2011**, *13*, 15681.

(27) Nieminen, J. J.; Hatay, I.; Ge, P. Y.; Mendez, M. A.; Murtomaki, L.; Girault, H. H. *Chem. Commun.* **2011**, *47*, 5548.

(28) Booth, S. G.; Uehara, A.; Chang, S. Y.; Mosselmans, J. F. W.; Schroeder, S. L. M.; Dryfe, R. A. W. *J. Phys. Chem. C* **2015**, *119*, 16785.

(29) Samec, Z. *Electrochim. Acta* **2012**, *84*, 21.

(30) Dryfe, R. A. W.; Uehara, A.; Booth, S. G. *Chem. Rec.* **2014**, *14*, 1013.

(31) Rodgers, A. N. J.; Booth, S. G.; Dryfe, R. A. W. *Electrochem. Commun.* **2014**, *47*, 17.

(32) Cheng, Y.; Schiffrin, D. J. *J. Chem. Soc., Faraday Trans.* **1996**, *92*, 3865.

(33) Uehara, A.; Hashimoto, T.; Dryfe, R. A. W. *Electrochim. Acta* **2014**, *118*, 26.

(34) Farges, F.; Sharps, J. A.; Brown, G. E. *Geochim. Cosmochim. Acta* **1993**, *57*, 1243.

(35) Chen, X.; Chu, W. S.; Chen, D. L.; Wu, Z. H.; Marcelli, A.; Wu, Z. Y. *Chem. Geol.* **2009**, *268*, 74.

(36) Paclawski, K.; Zajac, D. A.; Borowiec, M.; Kapusta, C.; Fitzner, K. *J. Phys. Chem. A* **2010**, *114*, 11943.

(37) Gaudet, J.; Bando, K. K.; Song, Z.; Fujitani, T.; Zhang, W.; Su, D. S.; Oyama, S. T. *J. Catal.* **2011**, *280*, 40.

(38) Ma, Q.; Divan, R.; Mancini, D. C.; Keane, D. T. *J. Phys. Chem. A* **2008**, *112*, 4568.

(39) Chang, S. Y.; Uehara, A.; Booth, S. G.; Ignatyev, K.; Mosselmans, J. F. W.; Dryfe, R. A. W.; Schroeder, S. L. M. *RSC Adv.* **2015**, *5*, 6912.

(40) Yao, T.; Sun, Z. H.; Li, Y. Y.; Pan, Z. Y.; Wei, H.; Xie, Y.; Nomura, M.; Niwa, Y.; Yan, W. S.; Wu, Z. Y.; Jiang, Y.; Liu, Q. H.; Wei, S. Q. *J. Am. Chem. Soc.* **2010**, *132*, 7696.

(41) Ohyama, J.; Teramura, K.; Higuchi, Y.; Shishido, T.; Hitomi, Y.; Kato, K.; Tanida, H.; Uruga, T.; Tanaka, T. *ChemPhysChem* **2011**, *12*, 127.

(42) Ohyama, J.; Teramura, K.; Higuchi, Y.; Shishido, T.; Hitomi, Y.; Aoki, K.; Funabiki, T.; Kodera, M.; Kato, K.; Tanida, H.; Uruga, T.; Tanaka, T. *Phys. Chem. Chem. Phys.* **2011**, *13*, 11128.

(43) Ma, J. Y.; Zou, Y.; Jiang, Z.; Huang, W.; Li, J.; Wu, G. Z.; Huang, Y. Y.; Xu, H. J. *Phys. Chem. Chem. Phys.* **2013**, *15*, 11904.

(44) Usher, A.; McPhail, D. C.; Brugger, J. *Geochim. Cosmochim. Acta* **2009**, *73*, 3359.

(45) Olaya, A. J.; Méndez, M. A.; Cortes-Salazar, F.; Girault, H. H. *J. Electroanal. Chem.* **2010**, *644*, 60.

(46) Zhou, M.; Gan, S. Y.; Zhong, L. J.; Dong, X. D.; Ulstrup, J.; Han, D. X.; Niu, L. *Phys. Chem. Chem. Phys.* **2012**, *14*, 3659.

(47) Kakiuchi, T. Equilibrium electric potential between two immiscible electrolyte solutions. In *Liquid-Liquid Interfaces Theory and Methods*; Volkov, A. G., Deamer, D. W., Eds.; CRC Press: Boca Raton, FL, 1996; Chapter 1.

(48) Duong, Q.; Tan, Y. S.; Corey, J.; Anz, S.; Sun, P. *J. Phys. Chem. C* **2015**, *119*, 10365.

(49) Mirceski, V.; Aleksovska, A.; Pejova, B.; Ivanovski, V.; Mitrova, B.; Mitreska, N.; Gulaboski, R. *Electrochem. Commun.* **2014**, *39*, 5.

(50) Hotta, H.; Akagi, N.; Sugihara, T.; Ichikawa, S.; Osakai, T. *Electrochem. Commun.* **2002**, *4*, 472.

(51) E, X. T. F.; Zhang, Y.; Zou, J. J.; Zhang, X. W.; Wang, L. *Mater. Lett.* **2014**, *118*, 196.

(52) Yoshida, Y.; Yoshida, Z.; Aoyagi, H.; Kitatsuji, Y.; Uehara, A.; Kihara, S. *Anal. Chim. Acta* **2002**, *452*, 149.

(53) Taylor, G.; Girault, H. H. J. *J. Electroanal. Chem. Interfacial Electrochem.* **1986**, *208*, 179.

(54) Osborne, M. C.; Shao, Y.; Pereira, C. M.; Girault, H. H. *J. Electroanal. Chem.* **1994**, *364*, 155.

(55) Ohde, H.; Uehara, A.; Yoshida, Y.; Maeda, K.; Kihara, S. *J. Electroanal. Chem.* **2001**, *496*, 110.

(56) Parker, A. J. *Chem. Rev.* **1969**, *69*, 1.

(57) Mosselmans, J. F. W.; Quinn, P. D.; Dent, A. J.; Cavill, S. A.; Moreno, S. D.; Peach, A.; Leicester, P. J.; Keylock, S. J.; Gregory, S. R.; Atkinson, K. D.; Rosell, J. R. *J. Synchrotron Radiat.* **2009**, *16*, 818.

DOI: 10.1021/jacs.5b07825
J. Am. Chem. Soc. 2015, 137, 15135−15144

(58) Dent, A. J.; Cibin, G.; Ramos, S.; Smith, A. D.; Scott, S. M.; Varandas, L.; Pearson, M. R.; Krumpa, N. A.; Jones, C. P.; Robbins, P. E. *B18: A core XAS spectroscopy beamline for Diamond in 14th J. Phys. Conf. Ser.* **2009**, *190*, 012039.
(59) Ravel, B.; Newville, M. *J. Synchrotron Radiat.* **2005**, *12*, 537.
(60) Schneider, C. A.; Rasband, W. S.; Eliceiri, K. W. *Nat. Methods* **2012**, *9*, 671.

DOI: 10.1021/jacs.5b07825
J. Am. Chem. Soc. 2015, 137, 15135−15144